Directional Filter for Tree Ring Detection

Rémi Decelle[1], Phuc Ngo[2], Isabelle Debled-Rennesson[2], Frédéric Mothe[3] and Fleur Longuetaud[3]
[1]*Univ. Lyon, Univ. Lyon 2, CNRS, INSA Lyon, UCBL, LIRIS, UMR5205, France*
[2]*Université de Lorraine, CNRS, LORIA, UMR 7503, Vandoeuvre-lès-Nancy, F-54506, France*
[3]*Université de Lorraine, AgroParisTech, INRAE, SILVA, F-54000 Nancy, France*

Keywords: Polar Quad-Tree Decomposition, Confidence Map, Tree Ring Width Estimation, Cross-Section Wood Image.

Abstract: This paper presents an approach to automatically detect tree rings and subsequent measurement of annual ring widths in untreated cross-section images. This approach aims to offer additional insights on wood quality. It is composed of two parts. The first one is to detect tree rings by using *directional filters* together with an adaptive refining process allowing to extract the rings from radial information for different angles around the tree pith. The second step consists in building a *confidence map* by considering polar quad-tree decomposition which enables us to identify the relevant regions of image for conducting the tree ring width measurements.The method is evaluated on two public datasets, demonstrating good performance in both detection and measurement. The source code is available at https://gitlab.com/Ryukhaan/treetrace/-/tree/master/treerings.

1 INTRODUCTION

Measuring tree rings of wood cross-sections is widely used to study tree growth. By measuring and dating all the tree rings from the center of the tree (pith) toward the bark, it is possible to reconstruct the past life of the tree and make assumptions about its growth conditions, including climate. Tree-rings are traditionally hand-measured, a process that demands significant time and human effort. In the past, several studies have been proposed for automating the detection of tree rings using computer vision techniques (e.g., (Conner et al., 1998; Laggoune et al., 2005)). However, these methods work on well-prepared wood samples and function in a semi-automatic manner.

In this work, we are interested in automatic tree ring analysis on color images of rough and untreated log ends (see Figure 1). Such images may exhibit disturbances like blurring, sawing marks or ambient light variations, which make the analysis more challenging (see wood patches in Figure 2). Furthermore, tree ring detection remains an active research topic today because of the difficulty of detection on certain species, particularly hardwoods (e.g., oak, beech, alder).

Recent studies in this area are often based on deep learning approaches (e.g., (Fabijańska and Danek, 2018; Marichal et al., 2023b; Poláček et al., 2023)). Most of these methods work with radial cores or strips of wood which provide partial information about the tree-ring structure. Nevertheless, growth rings can also be measured on a more macro scale, utilizing entire wood cross-section images, with the aim of providing information about the wood's quality. For soft-

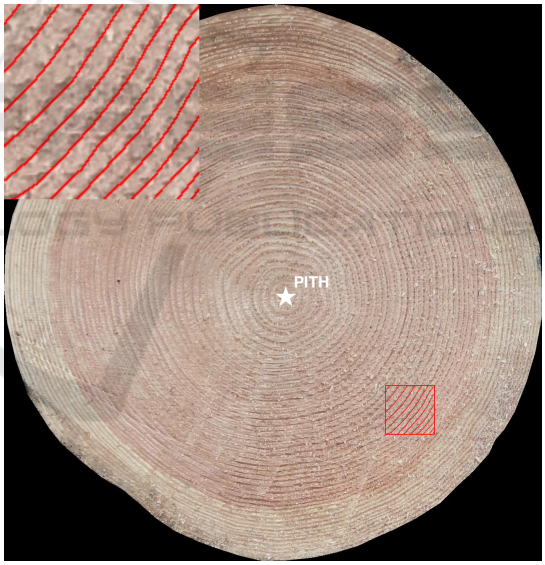

Figure 1: Rough wood cross-section RGB image.


Figure 2: Exhibit disturbances of wood cross-section.

Decelle, R., Ngo, P., Debled-Rennesson, I., Mothe, F. and Longuetaud, F.
Directional Filter for Tree Ring Detection.
DOI: 10.5220/0012457000003654

In *Proceedings of the 13th International Conference on Pattern Recognition Applications and Methods (ICPRAM 2024)*, pages 852-859
ISBN: 978-989-758-684-2; ISSN: 2184-4313

woods (e.g., Douglas fir, pine, spruce), narrow rings are generally associated with a good mechanical quality for use in construction and therefore also have an influence on the price of wood.

This article addresses the automatic measurement of growth rings, for use in forests or sawmills, to enable better quality assessment of logs. This work describes a method to automatically detect tree rings on segmented untreated log images by taking advantage of general structure of tree cross-sections. More precisely, the method utilizes directional filters together with an adaptive refining process to extract tree rings from radial information for different angles around the pith. From the detected tree rings, we generate a *confidence map* by considering polar quad-tree decomposition of the input image. This map enables us to identify the most relevant regions of image for conducting measurements, such as tree ring widths. The method is evaluated on two public datasets (Longuetaud et al., 2022; Marichal et al., 2023b) containing untreated cross-sectioned wood images. Comparisons are made with recent deep-learning approaches (Chen et al., 2018) to demonstrate its good performance in both detection and measurement. The source code is available at https://gitlab.com/Ryukhaan/treetrace/-/tree/master/treerings.

2 RELATED WORKS

In this section, we summarize existing algorithms applied on comparable unprepared images, resembling those examined in this paper. In particular, our focus is primarily on recent algorithms that might be particularly relevant to our specific case. More details of various methods for tree ring detection can be found in (Marichal et al., 2023b, Section 2).

(Fabijańska and Danek, 2018) proposed an automatic tree-ring boundary detector built upon the U-Net convolutional network. The proposed method focuses on wood core samples of tree ring porous species. They achieved a precision of 97% and a recall of 96%. It is mentioned that the tree-ring boundaries are accurately aligned with the real ones. However, minimal manual adjustments are needed, primarily around the pith, where tree-ring boundaries are less distinct, displaying varying tilts and orientations. Besides, they exclusively utilized core wood images rather than full cross-sections of tree log ends.

(Makela et al., 2020) proposed automated methods for locating the pith (center) of a tree disk, and ring boundaries. The proposed methods are based on combination of standard image processing techniques and tools from topological data analysis. However, these methods were assessed using 2D slices from 3D X-ray CT images of cross-sectioned tree trunks. Neither the code nor the data are publicly available.

(Gillert et al., 2023) addressed the problem of detecting tree rings on whole cross-section images as an instance segmentation task. For that, they proposed an iterative method, called *Iterative Next Boundary Detection (INBD)*. More precisely, an input image is passed through a semantic segmentation network that detects 3 classes: background, ring boundaries and ring center. Then, a polar grid is sampled starting from the detected ring center and passed to the INBD network to detect the next ring. The latter is repeated until the background is encountered. Their method was exclusively applied to microscopy images.

(Poláček et al., 2023) presented a supervised Mask R-CNN for detection and measurement of tree-rings from coniferous species. The CNN was trained and validated on RGB images of cross-dated microtome-cut conifers, with over 8000 manually annotated rings. Different pre- and post-processing have been applied to improve the model accuracy. They obtained a precision of 94.8% and a recall of 98.7% compared to cross-validated human detection. However, as most of the reviewed results, the approach works on cores rather than the whole cross-section.

(Marichal et al., 2023b) introduced a novel non-deep-learning approach to describe rings. A ring is composed of *nodes* linked between them which create a *chain*. A *node* is always on ray outwards from the pith. A *chain* is a ring if it is closed. All rings form a set called a *spider web*. Their definition allows to fit better tree rings. Their approach focuses on creating the *spider web* which is the closest to the rings on the cross-section image. Their results show a F-score of 89% on the UruDendro dataset (Marichal et al., 2023a). However, the cross-section were smoothed with a handheld planer and a rotary sander, meaning that the cross-section is not raw. Their code is publicly available.

3 METHOD

Our tree-ring detection (TRD) algorithm is based on directional approach. Indeed, rings are roughly concentric, even if their shape is irregular (mainly at the border of the log). This leads to the following characteristics:

- Two rings will never overlap;
- A ray traced outwards from the pith will cross each ring only once;
- A ring is delimited by two edges.

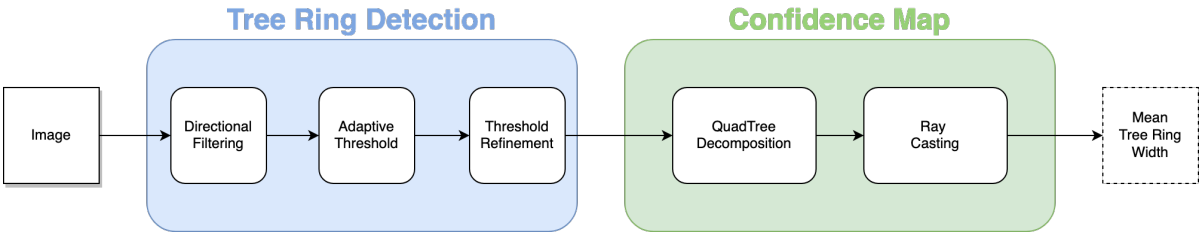

Figure 3: The global overview of our method.

Our method is compose of two parts. The first one focuses on TRD. The second one will estimate regions where the detection should be good enough to process some measurements, e.g., mean of tree ring widths. The big picture of our method is shown in Figure 3. The key feature of our proposal is that TRD and estimation are separated, allowing to easily replace either step in future works.

3.1 Tree Ring Detection (TRD)

In order to delineate tree rings, we assume that the log end image is segmented (Decelle et al., 2023; Wimmer et al., 2021). First, the input RGB image is converted into grayscale using usual formulae.

The next step aims at highlighting tree ring transitions and reducing noisy using directional filters. For this, we assume that the pith position is known. Automatic algorithms have already been proposed for this task (Norell and Borgefors, 2008; Kurdthongmee, 2020; Decelle et al., 2022).

3.1.1 Directional Filtering

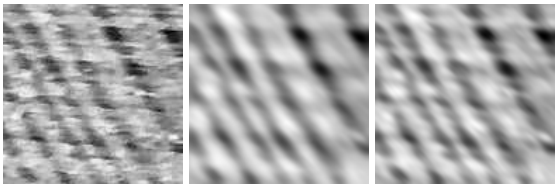

(a) Input image (b) Lorentz (c) Gaussian

Figure 4: One example to highlight the choice of Lorentz function instead of Gaussian function in Equation 2. Tree rings are more connected with the Lorentz function than gaussian function.

At first, we need a filter that preserve edges of the input image I, i.e. it preserves the ring boundaries. In order to reduce noise along the tangential direction of tree rings, we consider a modified directional Gaussian filter. The standard Gaussian domain kernel exhibits symmetry relative to the window center. To address the smoothing of image structures while incorporating orientation and anisotropy, we use an oriented kernel inspired by (Venkatesh and Seelamantula, 2015). Let $p = (p_x, p_y) \in I$ be the pixel to update and $q = (q_x, q_y) \in \mathcal{V}(p)$ be pixels in its neighborhood. In practice, $\mathcal{V}(p)$ is a window of size $n \times n$ pixels.

$$I'(p) = \sum_{q \in \mathcal{V}(p)} f(p-q)\, I(q_x - p_x, q_y - p_y) \quad (1)$$

where

$$f = \frac{1}{1 + \frac{x_\theta}{\sigma_x} + \frac{y_\theta}{\sigma_y}} \quad (2)$$

with

$$x_\theta = (q_x - p_x)\cos(\theta) - (q_y - p_y)\sin(\theta)$$
$$y_\theta = (q_x - p_x)\sin(\theta) + (q_y - p_y)\cos(\theta)$$

and θ is the angle between p and the pith c.

$$\theta = \arctan\left(\frac{p_y - c_y}{p_x - c_x}\right) \quad (3)$$

The parameters σ_x and σ_y control the kernel width in x-axis and y-axis, respectively. We used the Lorentz function $\frac{1}{1+x^2}$ over a Gaussian function because the former one is more spread in the direction θ than the latter one. This allows to filter more in the direction of θ than using a Gaussian. Figure 4 shows the difference between the Lorentz and Gaussian function with same pamareters for both. We can observe that tree rings show better connection characteristics with Lorentz than with a Gaussian function. Figure 5 shows an example of the result obtained with the proposed directional filter.

This filter is also interesting for its computational efficiency. Since the kernel has to be computed for each pixel, having a fast kernel computation is needed. Moreover, reducing time for filtering will allows us to spend more time in selection area for measuring tree ring widths (see Section 3.2).

3.1.2 Adaptive Threshold

After the filtering, we need to find the tree ring boundary. This is done by two steps: the filtered image is first thresholded, then the result is refined. We propose to use a fast threshold: adaptive mean threshold (Gonzalez, 2009). The threshold value is the mean of the neighbourhood intensity minus a constant C. An example is given in Figure 6 (left).

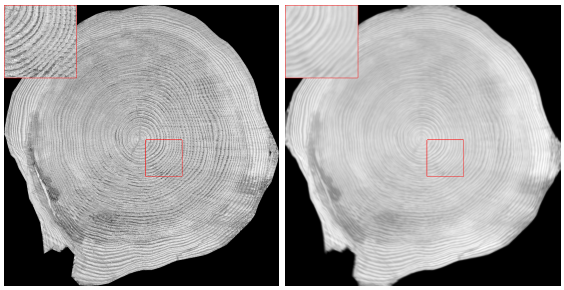

Figure 5: Left: Grayscale image. Right: Filtered image. At the top left of the images, a zoom of the red rectangle.

Figure 6: Left: Raw thresholded image. Right: Thresholded image after removing small areas.

3.1.3 Thinning

The previous adaptive threshold leads to thick tree rings. In order to make them thinner, we suggest the following steps. We remove all small connected components. Since such components have not enough information to estimate tree rings widths. For that, we first apply dilatation morphology in order to reconnect the regions. Then, if a region has less than 200 pixels, it is removed. This is illustrated in Figure 6 (right).

Finally, we focus on transitions from latewood (low intensity) to earlywood (high intensity) from the pith outwards (i.e. from the pith to the bark). It corresponds to a transition between white and black pixels according to the outward direction from the pith. A result of the thinning process is given in Figure 7.

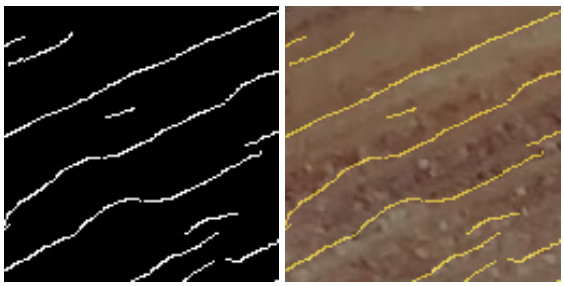

Figure 7: Left: Result obtained after thinning the previous thresholded image. Right: Delineation over the raw RGB image.

3.2 Confidence Map (CM)

Instead of trying to fully reconnect the detected segments to form closed rings, we propose here to partition the images into regions. We aim to identify the most relevant regions to make measurements. For that we will attribute a confidence value to each region, which will be seen as a confidence map (CM).

3.2.1 Polar Quad-Tree Decomposition

Since tree rings are close to concentric circles, we decide to split the image according to a polar quad-tree decomposition. Such a decomposition is well-known to decompose an image into regions in a recursive way. This technique reveals information about the image structure, and in our case, the information about how well tree rings have been segmented.

The pith is the center of the decomposition. The first (and biggest) region is a circle with the pith as center and a radius covering the cross-section. There are three conditions to stop the subdivision process:

1. the region should be not too large to estimate some directional characteristics. So, we suggest to split until the tree depth reaches ρ_{min};
2. the region should be not too small in order to have significant measurements. This purpose is done by stop splitting if the depth is greater than ρ_{max};
3. finally, the orientations in each region are all homogeneous.

Indeed, even if the detected tree rings are not globally connected, at a local level they are. Then, the orientations should be homogeneous in such region. This is why we choose the third criterion to stop or continue the subdividing.

To estimate local orientations, we use discrete geometry. More precisely, the tool proposed in (Decelle et al., 2021). However, this method is a little bit time-consuming. Therefore, we decide to apply it for d random selected points in each region. Each point provides us a set of orientations.

At the end, we obtain N_d possible orientations θ_i. The homogeneous criterion is the variance of those orientations. Set:

$$S = \frac{1}{N_d} \sum_{i=1}^{i=N_d} \sin(2\theta_i)$$

and

$$C = \frac{1}{N_d} \sum_{i=1}^{i=N_d} \cos(2\theta_i)$$

The variance is computed as follows:

$$R = \sqrt{\bar{S}^2 + \bar{C}^2}$$

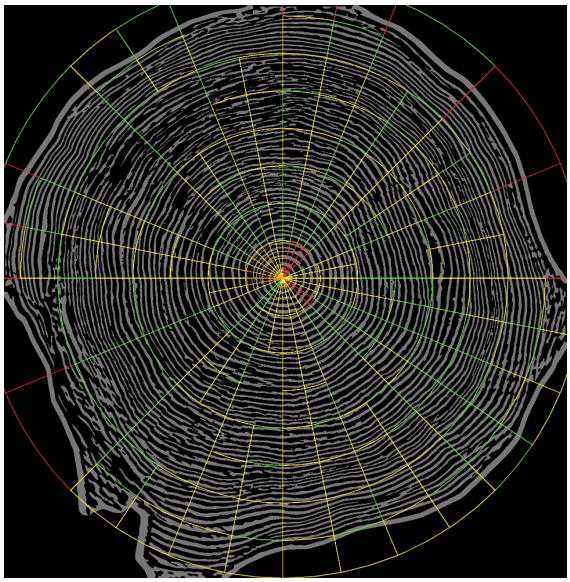

Figure 8: Example of polar quad-tree decomposition. We show non-thin segmentation to hightlight link between segmentation and evaluated confidence.

By definition, R is in range of 0 and 1. This allows us to interpret the value as a quality of the region. If all θ_i are the same, then $S^2 + C^2 = 1$, then $R = 1$. It defines the confidence value of the current region. A region will be split if its variance is lower than ε, meaning that the region is not enough homogeneous.

Figure 8 shows the proposed method of image decomposition to provide a confidence map. Green regions are reliable regions, i.e. $R \geq \varepsilon$. Orange regions have a value of $\varepsilon > R \geq \frac{\varepsilon}{2}$. And red regions have a value of $R < \frac{\varepsilon}{2}$. In this figure, $\varepsilon = 0.98$.

4 EXPERIMENTS AND RESULTS

4.1 Datasets

To test the proposed method, we consider two datasets:

1. The dataset (Longuetaud et al., 2022) from which 6 images have the tree-rings being fully and manually delineated. Plus 62 images in a core-style (see Figure 10 were created and manually segmented in this dataset.
2. The UruDendro dataset (Marichal et al., 2023a), which is available online and composed of cross-section images of *Pinus taeda* species from northern Uruguay, ranging from 13 to 24 years old. It has a total of 64 images at different resolutions. Pith positions are also given.

4.2 Metrics

To evaluate the method and compare with the others, we consider 2 different metrics. First one is to evaluate the tree ring widths, since it is the criteria most often used for qualifying tree growth. However, such measurements do not evaluate the quality of the delineation. Thus, we have to determine whether the detected rings are closed to the ground truths by assigning them to the closest ground truth rings and compute a distance metric for the detection's quality.

4.2.1 Tree Ring Widths

The tree ring widths are directly correlated to wood quality. In each image, we obtain an estimated mean tree ring width, denoted as $\hat{y}$. Afterwards, standard metrics can be calculated to assess the accuracy of the estimated mean of the tree ring widths:

$$RMSE = \sqrt{\frac{1}{n}\sum_i (\hat{y}_i - y_i)^2}$$

$$Biais = \frac{1}{n}\sum_i (\hat{y}_i - y_i)$$

$$Err = \frac{RMSE}{\frac{1}{n}\sum_i y_i}$$

4.2.2 Hausdorff Distance

From a computer vision point of view, the mean width measurement alone does not convey the accuracy of the tree ring segmentation. Specifically, a uniform shift in all ring boundaries does not change the mean width. Consequently, to assess the segmentation quality, we rely on an alternative metric.

First, for every detected tree ring, we link it to the nearest ground truth ring. We measure the distance between the ring boundary and the ground truth based on the average Hausdorff distance (Aydin et al., 2021). Given two sets A and B, the Hausdorff distance between these two sets is calculated as follows:

$$d(A,B) = \frac{1}{|A|}\sum_{a \in A} d(a,B)$$

where

$$d(a,B) = \min_{b \in B}(d(a,b))$$

The distance between two points is computed with the euclidean distance:

$$d(a,b) = ||a-b||_2$$

Finally, the mean Hausdorff distance is computed as follows:

$$d_{haus}(A,B) = \frac{1}{2}(d(A,B) + d(B,A))$$

Our evaluation metric is the mean for all rings:

$$\bar{D}_{hauss} = \frac{1}{n}\sum_{i=1}^{n} d_{haus}(A_i, B_i) \quad (4)$$

4.3 Experiments

This section presents several experiments to understand and highlight the method and its limitations. The following table 1 sums up all parameter values used in experiments for our method.

Table 1: Summary of TRD and CM parameter values used.

TRD param.	σ_x	σ_y	n	*window*	C
	1.0	5.0	$3\sigma_x + 1$	31	2
CM param.	ρ_{min}	ρ_{max}	N	ε	
	3	4	10	0.98	

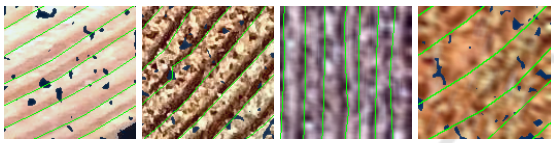

Figure 9: Examples of training images of size 128×128 pixels. Targeted TRD are shown in green.

4.4 Neural Network

We aim to conduct a comparative analysis between our method and deep-learning approaches. For that, we have also trained DeepLabV3Plus for tree ring segmentation (Chen et al., 2018) with ResNet-101 (He et al., 2016) as backbone and pre-trained on imagenet (Russakovsky et al., 2015).

We have 6 (over 208) images from (Longuetaud et al., 2022) and 4 (over 64) images from Urudendro dataset (Marichal et al., 2023a). The images were spitted into patches of size 128×128 pixels, which lead to 8537 patches in total. We use data augmentation with a dihedral group of eight orientations (D8) and several blur (motion, gaussian, and so on). The training set has 80% of images and validation set has 20% of images. The test set is composed of unsegmented images from (Longuetaud et al., 2022) dataset and images not included for the training in Urudendro dataset. Figure 9 shows some examples of images used for training and validation. We have ordered the images, in our point of view, from easiest to the most difficult to segment.

The network operates by taking image patches and generating predictions based on the small local windows. However, this approach may result in higher prediction errors, in particular, near the borders of the patches. It is worsen when concatenating the predictions and leading to disconnected and/or incoherent tree ring segmentation.

A potential solution involves adjusting the sizes of inputs and outputs during training, utilizing a large neural network during testing. Yet, implementing such a strategy is challenging and not memory friendly. A more straightforward solution is to use some 2D interpolation between overlapping patches of final predictions. This is our adopted approach.

First, we use overlapping patches to have different global context for the same tree rings. We propose a 50% overlap of patches, which is a good compromise between inference time and reduction of undesirable side effects. Second, we use rotations and mirrors, so as to make the neural network view the image under several different angles (using dihedral group of eight orientations called D8 as used for data augmentation). The 8 predictions are then averaged, and thus reduces variance in predictions.

4.5 Results

Table 2: Values of RMSE, Biais and Percentage error (Err). Values are in mm for (Longuetaud et al., 2022) and in pixels for (Marichal et al., 2023a). CM indicates if Confidence Map has been included or not.

	CM	RMSE	Biais	Err
Logyard (in mm)				
Our method	✓	**0.830**	-0.441	**0.148**
Our method		0.962	**-0.034**	0.171
DeepLabV3+	✓	1.082	-0.702	0.212
DeepLabV3+		1.445	-0.019	0.257
Urudendro (in pixels)				
Our method	✓	14.626	-5.316	0.281
Our method		16.879	-15.175	0.325
DeepLabV3+	✓	**12.886**	**-3.16**	**0.248**
DeepLabV3+		16.006	3.986	0.308

We perform the whole method on each mentioned dataset (Section 4.1). We also perform an ablation study to evaluate the interest of each part (TRD and CM). More precisely, we perform TRD alone, TRD combined with CM, DeepLabV3+ alone and DeepLabV3+ combined with CM. Section 2 shows the values of RMSE, bias, and the percentage of error for each experiments (Section 4.2.1).

First, we can observe that processing the confidence map increases the quality of the estimation. On the Urudendro dataset, confidence map combined with deep learning provides the best results. However, deep learning method is less accurate on (Longuetaud et al., 2022) dataset. An explication is that 4 over 64 images from Urudendro dataset have been used for training and only 6 over 208 images have been used for (Longuetaud et al., 2022) dataset. This leads to an imbalance training set. Furthermore, there are more

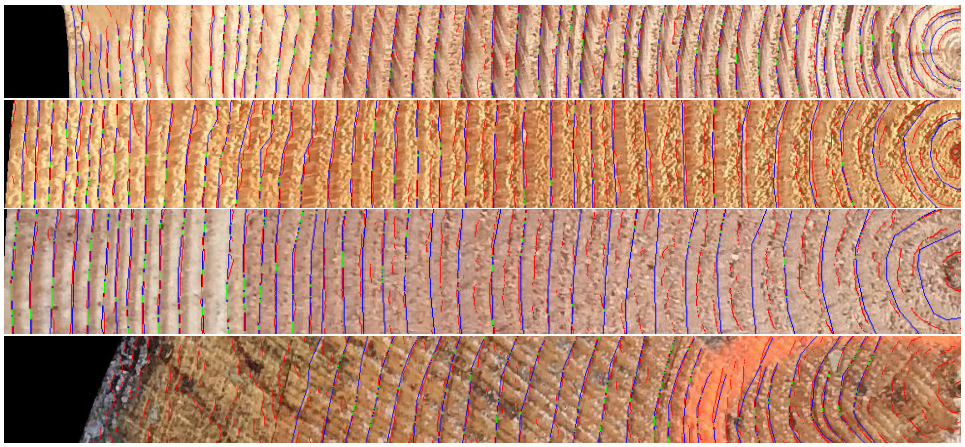

Figure 10: Four examples of extracted sub-images to assess the segmentation quality. Blue lines are ground truth, red lines are predicted boundaries and green lines are boundaries where predicted and ground truth match.

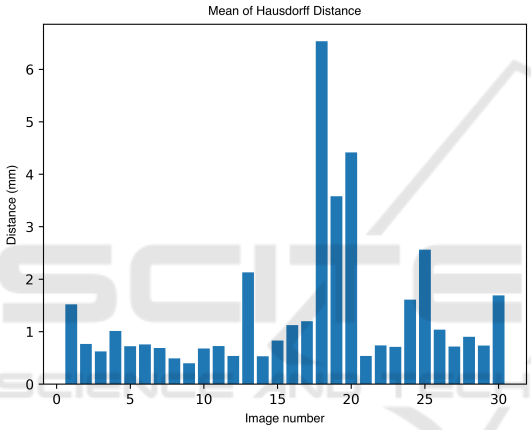

Figure 11: Mean Hausdorff Distance for 30 sub-images with ground truths.

images similar to Figure 10 most-left and left than most-right and right in training set. Neural network learned to detect edges but struggled to detect boundaries when there are strong noises. Our method also struggles to detect such boundaries but, since the orientation is assumed to be known, strong noises are reduced.

Concerning the bias, it is -0.441 mm for (Longuetaud et al., 2022) dataset with confidence included and -0.034 mm without. Deep learning approach seems to overestimate the width. This could be due to not well-segmented tree rings. It detects less boundaries than our proposed method does (see Figure 10). Using the confidence map reduces the biais and sometimes even makes it negative. One explanation is that tree rings are more visible outwards the pith and are well-segmented, but those tree rings have smaller width than those close to the pith. This also explains why the bias is always negative.

Furthermore, these values should be considered in light of how the ground truth was obtained, for at least (Longuetaud et al., 2022) dataset. The ground truth was obtained from 4 orthogonal directions, while in our method, we potentially consider all possible directions. Additionally, the resolution of the processed images is not the same as that used for the ground truth. We cannot be more precise than a certain distance due to the image resolution. On average, one pixel is equivalent to 0.21 mm, meaning that a variation of one pixel results in a variation of around 3.75% from the ground truth.

Nonetheless, all these values are encouraging and support our method for both tree ring detection and confidence map. Some refinements should lead to better estimation.

As we already said, a good estimation of tree ring width does not imply a well delineation of tree rings. For this, we process two further measurements. However, having ground truth for the entire dataset is very challenging. Therefore, we have selected 30 subimages for segmentation assessment. These subimages are in core-style, i.e. we select one of the four directions then from the pith to the outwards (see Figure 10). Subimages are reoriented in order to always have the pith on the right. Each subimages has a height of 128 pixels. The ground truth is shown in blue while the detected tree rings is in red. Finally, in green, pixels where the estimation matches the ground truth are highlighted.

Figure 11 shows the mean Hausdorff distance depicted in Equation 4 for these 30 sub-images. The resulting mean is 1.349 mm, that is close the value of RMSE previously obtained. It is encouraging for the future works. Nevertheless, as already mentioned, the mean tree ring width of the whole image is not necessarily a great indicator of a good detection. For in-

stance, the image with highest d_{hauss} (a value of 6.523 mm) is obtained for the last image in Figure 10 and it is not the image with the highest mean tree ring width (a value of 11.988 mm). Results show that introducing a confidence map is relevant.

5 CONCLUSIONS

A new framework is presented by combining a directional filter to detect tree rings and a confidence map to perform measurements on detected tree rings. The method works on untreated cross-section wood images. Over the experiments, it achieves a RMSE of 0.830 mm for the (Longuetaud et al., 2022) dataset, slightly better than a deep learning method of 1.482 mm. We also obtained great results for Urudendro dataset (Marichal et al., 2023b) with a RMSE of 14.626 pixels. Note that combining the confidence map and deep learning offers also great results.

In future works, we will include automatic pith detection, cross-section segmentation, other tree species and other deep learning methods. We will also adapt our method to other applications where orientation plays an important role such as fingerprint images.

REFERENCES

Aydin, O. U., Taha, A. A., Hilbert, A., Khalil, A. A., Galinovic, I., Fiebach, J. B., Frey, D., and Madai, V. I. (2021). On the usage of average hausdorff distance for segmentation performance assessment: hidden error when used for ranking. *European radiology experimental*, 5:1–7.

Chen, L.-C., Zhu, Y., Papandreou, G., Schroff, F., and Adam, H. (2018). Encoder-decoder with atrous separable convolution for semantic image segmentation. In *Proceedings of ECCV*, pages 801–818.

Conner, W. S., Schowengerdt, R. A., Munro, M., and Hughes, M. K. (1998). Design of a computer vision based tree ring dating system. In *IEEE Southwest Symposium on Image Analysis and Interpretation (Cat. No. 98EX165)*, pages 256–261.

Decelle, R., Ngo, P., Debled-Rennesson, I., Mothe, F., and Longuetaud, F. (2021). Digital straight segment filter for geometric description. In *International Conference on Discrete Geometry and Mathematical Morphology*, pages 255–268.

Decelle, R., Ngo, P., Debled-Rennesson, I., Mothe, F., and Longuetaud, F. (2022). Ant colony optimization for estimating pith position on images of tree log ends. *Image Processing On Line*, 12:558–581.

Decelle, R., Ngo, P., Debled-Rennesson, I., Mothe, F., and Longuetaud, F. (2023). Light u-net with a new morphological attention gate model application to analyse wood sections. In *ICPRAM 2023*.

Fabijańska, A. and Danek, M. (2018). Deepdendro–a tree rings detector based on a deep convolutional neural network. *Computers and electronics in agriculture*, 150:353–363.

Gillert, A., Resente, G., Anadon-Rosell, A., Wilmking, M., and von Lukas, U. F. (2023). Iterative next boundary detection for instance segmentation of tree rings in microscopy images of shrub cross sections. In *Proceedings of IEEE CVFPR*, pages 14540–14548.

Gonzalez, R. C. (2009). *Digital image processing*. Pearson education india.

He, K., Zhang, X., Ren, S., and Sun, J. (2016). Deep residual learning for image recognition. In *Proceedings of IEEE CCVPR*, pages 770–778.

Kurdthongmee, W. (2020). A comparative study of the effectiveness of using popular dnn object detection algorithms for pith detection in cross-sectional images of parawood. *Heliyon*, 6(2).

Laggoune, H., Guesdon, V., et al. (2005). Tree ring analysis. In *IEEE Canadian Conference on Electrical and Computer Engineering*, pages 1574–1577.

Longuetaud, F., Pot, G., Mothe, F., Barthelemy, A., Decelle, R., Delconte, F., Ge, X., Guillaume, G., Mancini, T., Ravoajanahary, T., et al. (2022). Traceability and quality assessment of douglas fir (pseudotsuga menziesii (mirb.) franco) logs: the treetrace_douglas database. *Annals of Forest Science*, 79(1):1–21.

Makela, K., Ophelders, T., Quigley, M., Munch, E., Chitwood, D., and Dowtin, A. (2020). Automatic tree ring detection using jacobi sets. *arXiv preprint arXiv:2010.08691*.

Marichal, H., Passarella, D., Lucas, C., Profumo, L., Casaravilla, V., Rocha Galli, M. N., Ambite, S., and Randall, G. (2023a). UruDendro: An Uruguayan Disk Wood Database For Image Processing.

Marichal, H., Passarella, D., and Randall, G. (2023b). Cstrd: a cross sections tree ring detection method. *arXiv preprint arXiv:2305.10809*.

Norell, K. and Borgefors, G. (2008). Estimation of pith position in untreated log ends in sawmill environments. *Computers and Electronics in Agriculture*, 63(2):155–167.

Poláček, M., Arizpe, A., Hüther, P., Weidlich, L., Steindl, S., and Swarts, K. (2023). Automation of tree-ring detection and measurements using deep learning. *Methods in Ecology and Evolution*, 14(9):2233–2242.

Russakovsky, O., Deng, J., Su, H., Krause, J., Satheesh, S., Ma, S., Huang, Z., Karpathy, A., Khosla, A., Bernstein, M., Berg, A. C., and Fei-Fei, L. (2015). ImageNet Large Scale Visual Recognition Challenge. *International Journal of Computer Vision (IJCV)*, 115(3):211–252.

Venkatesh, M. and Seelamantula, C. S. (2015). Directional bilateral filters. In *Proceeding of IEEE ICASSP*, pages 1578–1582.

Wimmer, G., Schraml, R., Hofbauer, H., Petutschnigg, A., and Uhl, A. (2021). Two-stage cnn-based wood log recognition. In *International Conference on Computational Science and Its Applications*, pages 115–125.